5 Comprehensive Ultrasonographic Anatomy of the Normal Skin, Nail, Hair, and Adjacent Structures

Ximena Wortsman, Camila Ferreira-Wortsman, Yamile Corredoira, and Kharla Pizarro

Introduction

The knowledge of normal anatomy is essential for performing a good ultrasonographic examination. This chapter reviews the normal anatomy of the skin, hair, and adjacent structures using different frequencies but conserving the same study protocols.

X. Wortsman (✉)
Institute for Diagnostic Imaging and Research of the Skin and Soft Tissues, Santiago, RM, Chile

Department of Dermatology, Universidad de Chile, Santiago, RM, Chile

Department of Dermatology, Pontificia Universidad Catolica de Chile, Santiago, RM, Chile

C. Ferreira-Wortsman
School of Medicine, Universidad Finis Terrae, Santiago, Chile

Y. Corredoira
Department of Pathology, Dermopathology Section, Universidad de Chile, Santiago, Chile

K. Pizarro
Department of Pathology, Hospital San José, Santiago, Chile

Skin

The skin comprises three layers: epidermis, dermis, and hypodermis, also called subcutaneous tissue [1–3].

The **epidermis** usually appears as a hyperechoic line in the skin out of the palms and soles and as a bilaminar layer in the palms and soles. The echogenicity of the epidermis is due to the keratin of the stratum corneum. The epidermis's bilaminar appearance in the palms and soles is due to a thicker stratum corneum in these regions. At frequencies that go from 46 to 70 MHz, the epidermis presents a thin, intense hypoechoic band underneath the hyperechoic line of the stratum corneum, which corresponds to the non-stratum corneum layers (stratum lucidum, granulosum, spinosum, and basale). At 70 MHz, it is possible to detect within the palms and soles' epidermis hyperechoic slightly oblique bands that correspond to the sweat glands' secretory ducts [4–11].

The **dermis** shows as a hyperechoic band, and the collagen content gives its echogenicity. The aging and exposure to the sun generate glycosaminoglycans' deposits in the upper dermis, called elastosis. These photoaging signs produce a hypoechoic diffuse band called subepidermal low echogenic band (**SLEB**) in the upper dermis of the skin of sun-exposed regions such as the face, neck, or dorsum of the forearms. It is essen-

X. Wortsman (ed.), *Textbook of Dermatologic Ultrasound*,
https://doi.org/10.1007/978-3-031-08736-3_5

tial not to confuse the SLEB with inflammatory or infiltrative conditions [4–12].

The dermis is thinner in the face and ventral forearm and thicker in the dorsal and lumbar regions. This variable thickness of the dermis can explain why cutaneous tumors can more easily involve deeper layers such as muscle or cartilages in the facial region [4–12].

The **hypodermis, also called subcutaneous tissue**, appears as a hypoechoic band. The fatty tissue provides its echogenicity. Within the fatty lobules, there are hyperechoic linear and wavy fibrous septa. At 70 MHz, sometimes it is possible to observe protrusions, also called papillae, of the fatty subcutaneous tissue into the dermis in some corporal locations. The hypodermal fatty tissue is absent in the eyelids and lips as well as in the proximal part of the periungual region, also called the proximal nail fold [4–12].

At 15–46 MHz, usually, the machines detect subcutaneous vascularity but rarely the dermal vessels. However, at 70 MHz, it is possible to view the lower dermal (reticular) vessels in some areas. These vessels tend to show low velocity (≤15 cm/s) [4–13] (Figs. 5.1, 5.2, 5.3, 5.4, and 5.5).

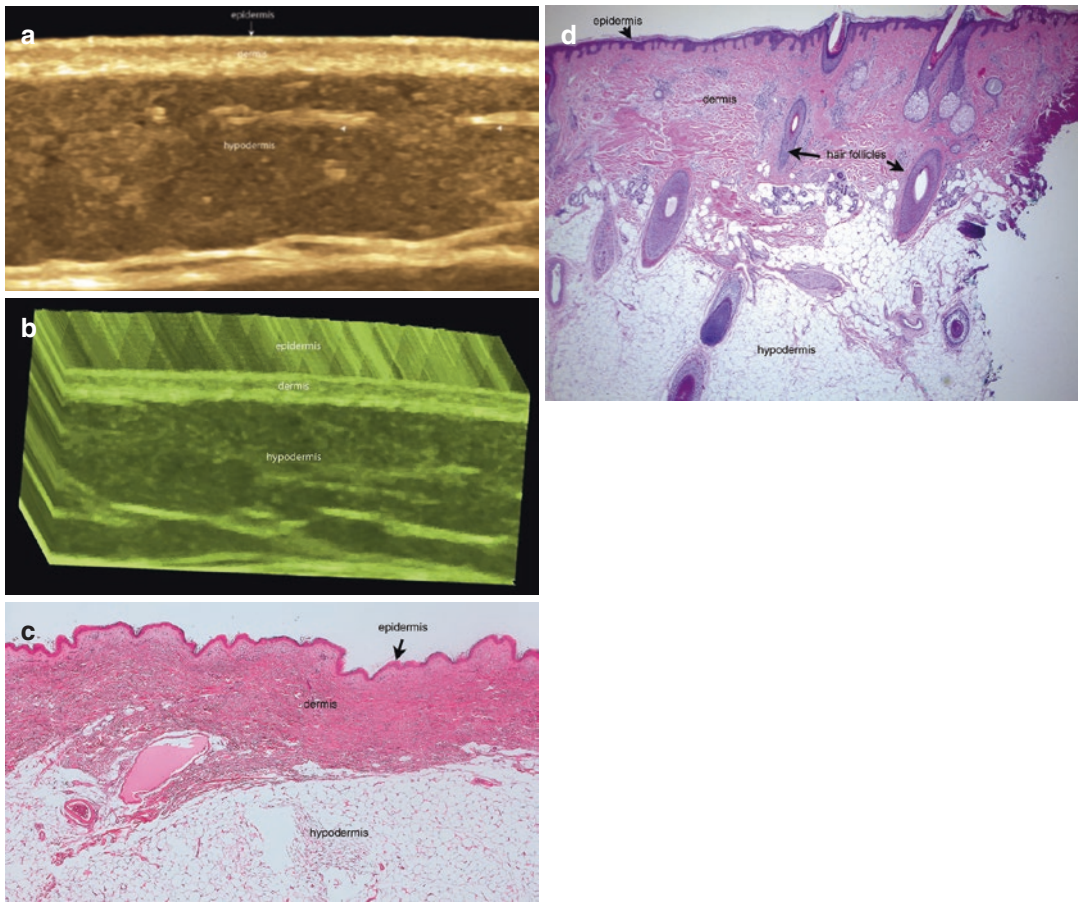

Fig. 5.1 (**a**) Normal skin layers (grayscale with a color filter at 18 MHz). (**b**) 3D reconstruction of grayscale with a color filter. Histology (hematoxylin and eosin). (**c**) Normal skin of the chest. (**d**) Normal skin of the scalp

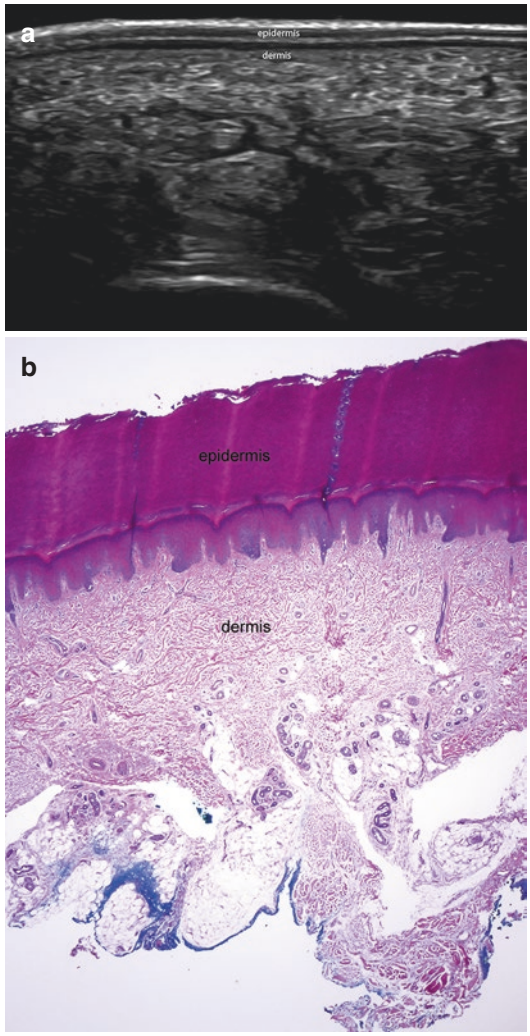

Fig. 5.2 (**a**) Grayscale ultrasound of the plantar skin at 24 MHz. Notice the bilaminar thick hyperechoic epidermis. (**b**) Histology (hematoxylin and eosin) of the plantar skin

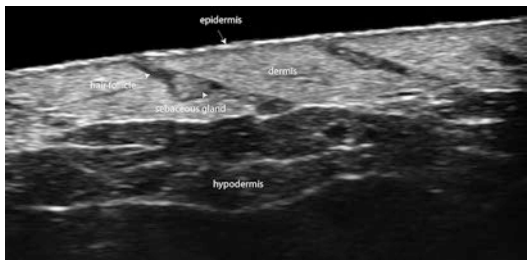

Fig. 5.3 Normal skin at 70 MHz. Notice the echostructure of the epidermis, dermis, hypodermis, hair follicle, and sebaceous gland

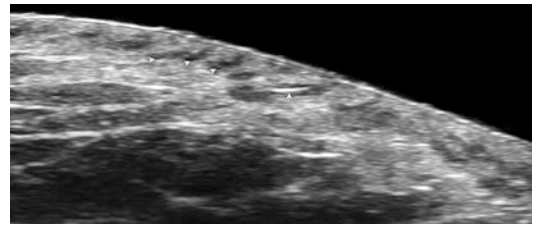

Fig. 5.4 Normal skin of the cheek at 70 MHz. It is possible to detect the tiny hair follicles in the dermis (oblique arrows). In one of them, you can notice a hyperechoic line that corresponds to a fragment of a hair tract (arrow pointing up)

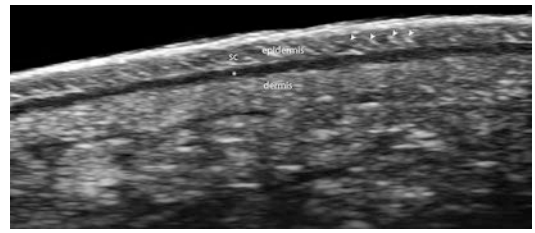

Fig. 5.5 The plantar skin at 70 MHz is composed of a thick hyperechoic band that corresponds to the stratum corneum (sc) and a thin hypoechoic basal layer that corresponds to the gathering (*) of the stratum lucidum granulosum, spinosum, and basale. Notice the oblique hyperechoic bands in the epidermis (arrows pointing down) that correlate with the sweat ducts. The dermis is also hyperechoic

Hair

The hair has two parts; one is the hair follicle located in the dermis, and the other one is the (hair shaft) that appears on the surface of the skin [2, 8, 9, 11, 14, 15].

The hair follicles show on ultrasound as hypoechoic oblique dermal bands. At 70 MHz, it is possible to detect the hair tract located inside the hair follicle before its exit to the surface in some regions. The hair tracts show two normal morphologies: in the scalp, most of the hair tracts present a trilaminar hyperechoic appearance composed of an outer cuticle-cortex complex and the inner medulla. The hair tracts show a bilaminar hyperechoic appearance in the rest of the body, also called "villus type" of hair, composed of an outer cuticle-cortex complex and without an inner medulla [6, 8, 9, 11, 14, 15].

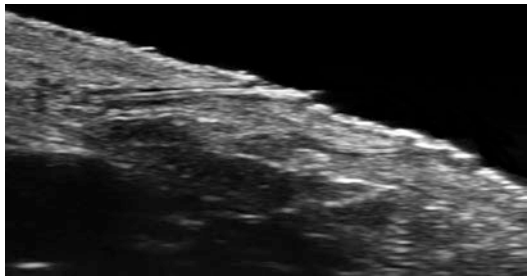

Fig. 5.6 Hair follicle and tract. The hair tract is seen as a bilaminar hyperechoic structure within the hair follicle

The eyelashes and the eyebrows appear as monolaminar hyperechoic structures, and at 70 MHz, it is possible to observe the eyelashes' hair follicles in the eyelid [6, 7, 9, 11, 15].

There are parts of the body that lack hair follicles, such as the palms and soles. This is relevant to evaluate the differential diagnosis of lesions located in those areas because hair-derived lesions are rare [7, 9, 11, 15].

The scalp's vascularity runs through a centripetal network that comes from the internal and external carotid arteries. The arteries are thicker in the periphery and thinner in the midline region [7, 9, 11, 15].

On ultrasound, it is possible to detect the **phases of the hair cycle** clock. The **anagen phase** is the active stage and shows the terminal hair follicle with a prominent bulb commonly occupying the whole dermis and upper hypodermis. The **telogen phase** is the resting phase and presents a short hair follicle located in the upper dermis. The **catagen phase** is the intermediate stage. The ultrasound discrimination of the hair's presence and growth stage might be significant in some hair conditions [6, 7, 9, 11, 15] (Fig. 5.6).

Additional Structures Detected at Ultrahigh Frequency (70 MHz)

Arrector Pili Muscle

At 70 MHz, and in some corporal regions, it is possible to detect the arrector pili muscle as a hypoechoic and oblique band attached to the hair follicle [8] (Fig. 5.7).

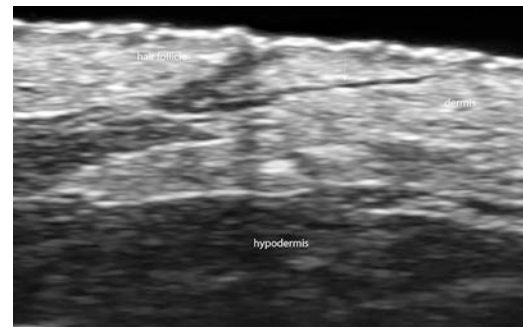

Fig. 5.7 Arrector pili muscle. Hypoechoic oblique band (arrow) located adjacent to the hair follicle (70 MHz)

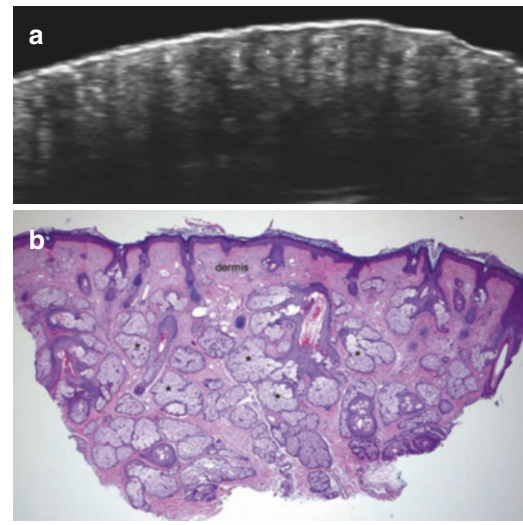

Fig. 5.8 Sebaceous glands. (**a**) Grayscale ultrasound (70 MHz). The sebaceous glands appear as hyperechoic oval-shaped dermal structures (*). (**b**) Histology (hematoxylin and eosin) presents the nasal skin. Notice the prominent sebaceous glands (*)

Sebaceous Glands

These glands are usually viewed with ultrahigh frequency (70 MHz) and appear as hyperechoic oval-shaped structures attached to the hair follicles. There are locations where these glands are more prominent such as in the face [8] (Fig. 5.8).

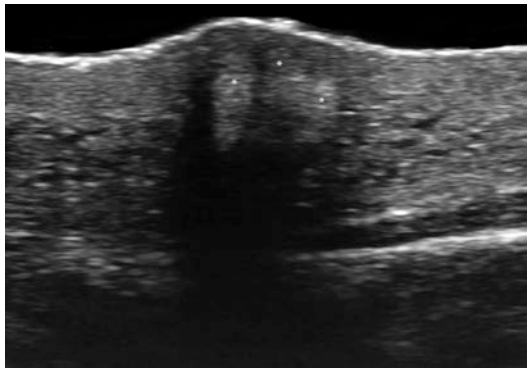

Fig. 5.9 Montgomery glands. These glands appear as clusters of hyperechoic oval-shaped dermal structures without prominent hair follicles in the periphery (70 MHz). Indeed, they are variants of sebaceous glands typically located in the areolar region.

Montgomery Glands

These glands are variants of sebaceous glands located in the nipple-areola region; therefore, at 70 MHz, they appear as clusters of hyperechoic oval-shaped structures attached to tiny hair follicles or not attached to hair follicles [8] (Fig. 5.9).

Apocrine Glands

These are sweat glands, usually located in the axillary and groin regions. The clusters of apocrine glands can be detected at 70 MHz. These show on ultrasound as round or oval-shaped mixed echogenicity structures with hypoechoic and anechoic lacunar areas that resemble an ovary's ultrasound appearance (pseudo-ovary sign) [8] (Fig. 5.10).

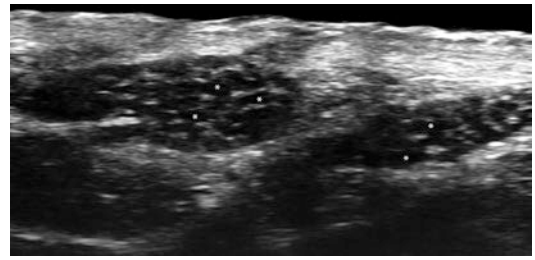

Fig. 5.10 Apocrine glands. Notice the round and oval-shaped lower dermal structures that show anechoic lacunar areas (*) that resemble an ovary structure, which is called the "pseudo-ovary" sign (70 MHz)

Nail

The nail unit presents three main regions on ultrasound: the nail plate, the nail bed, and the periungual region [5–7, 9, 16–19].

At 15–45 MHz, the nail plate usually appears as a bilaminar hyperechoic layer with an outer dorsal plate and an inner ventral plate. In between the plates, there is an anechoic interplate space. At >46–70 MHz, the interplate space becomes hyperechoic but still is less echogenic than the dorsal and ventral plate. The variable degrees of hyperechogenicity are provided by different keratin types within the nail plate, which is more evident at higher frequencies [5–7, 9, 19].

The nail bed shows as a hypoechoic space that turns to slightly hyperechoic underneath the matrix region located in the proximal part [5–7, 9, 19].

The proximal and lateral nail folds compose the periungual skin and present a similar echostructure to the epidermis and dermis located in other corporal regions; however, they do not contain fatty tissue. Conversely, the pulp of the finger shows a prominent fatty tissue [7, 9, 19].

There is a hyperechoic line underneath the nail bed that corresponds to the distal phalanx's bony margin [7, 9].

In the proximal part, it is possible to observe the anechoic space of the distal interphalangeal joint (or interphalangeal joint in the thumbs and big toes) and the extensor tendons' distal insertion with their hyperechoic fibrillar appearance [7, 9].

The nail's vascularity comes from the digital arteries of the fingers. It tends to show a higher concentration of vascularity in the deeper two-thirds of the nail bed, close to the bony margin. At 18–46 MHz, usually, there is a space without detectable blood flow in the upper third. This is due to the devices' detection threshold that commonly can detect velocities >2 cm/s. However,

on some high-end devices, it may be possible to observe superficial vessels in the nail bed. This could be more evident in power Doppler, echoangio, or microvascularity applications.

There are also variations in the nail and periungual region's vascularity according to the degree of peripheral vasoconstriction, which tends to be more prominent on the feet. Therefore, the blood flow on the toenails may be more challenging to catch than the fingernails. The application of warm gem may help to overcome this situation.

On ultrasound, it is impossible to see the matrix cells; however, the change in the nail bed's echogenicity in the proximal part can orient us to know the approximate location. The matrix of the nail is also present in the lateral parts called wings. The matrix wings' involvement can be relevant in some diseases that affect the nail plate's location [5–7, 9, 16, 18, 19] (Figs. 5.11 and 5.12).

Adjacent Normal Structures

Lymph Nodes

These appear as oval-shaped, mixed echogenicity structures that show a hypoechoic rim that corresponds to the cortex and a hyperechoic center that corresponds to the medulla.

On color or power Doppler, lymph nodes present centripetal vascularity mainly located in the medulla and inner cortex with a regular distribution of the vessels and an eccentric hilum that shows low-velocity arteries and veins (Fig. 5.13).

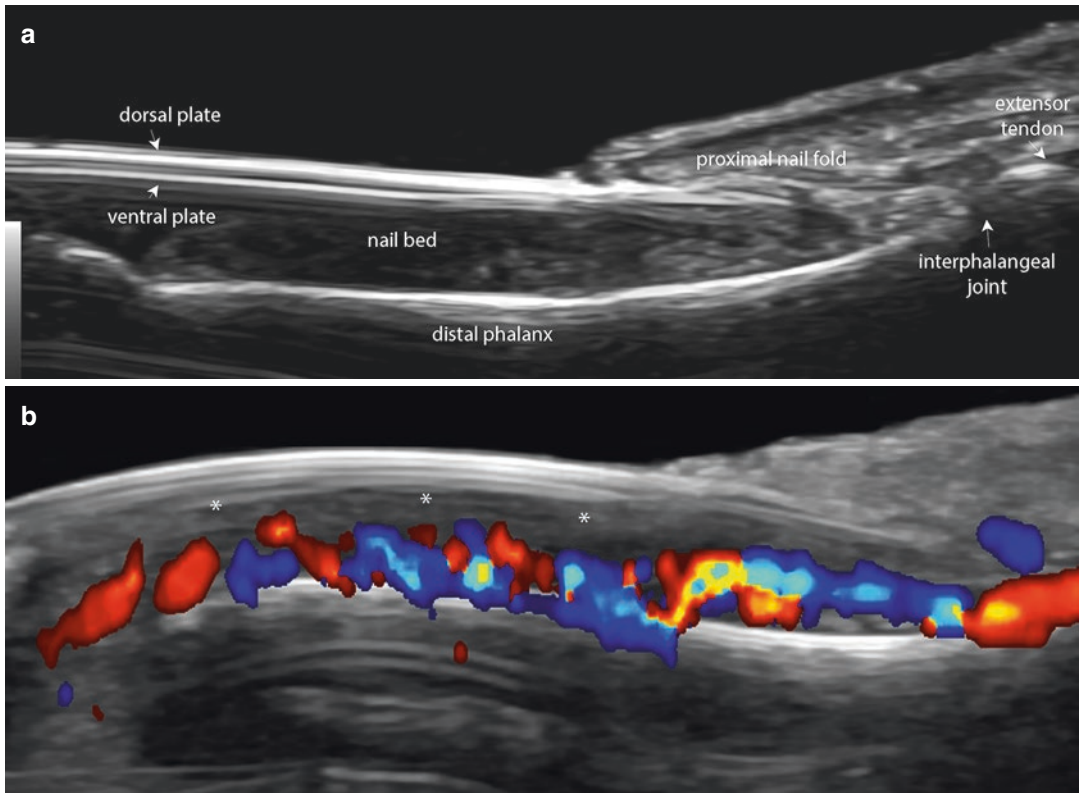

Fig. 5.11 Normal nail anatomy (longitudinal views). (**a**) Grayscale demonstrates the parts of the nail. (**b**) Color Doppler shows the blood flow within the nail bed. Notice that there is an empty, superficial space without detectable blood flow (*). This is due to the ungual vessels' location that is usually within the deep two-thirds of the nail bed, closer to the distal phalanx's bony margin

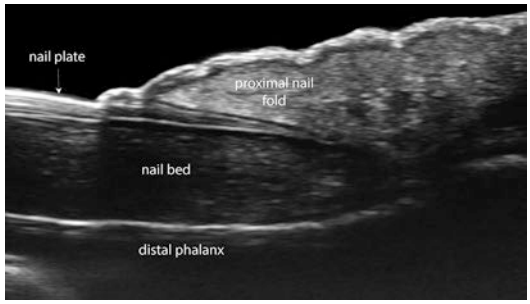

Fig. 5.12 Nail at 70 MHz. Grayscale (longitudinal view) shows the proximal part of the nail

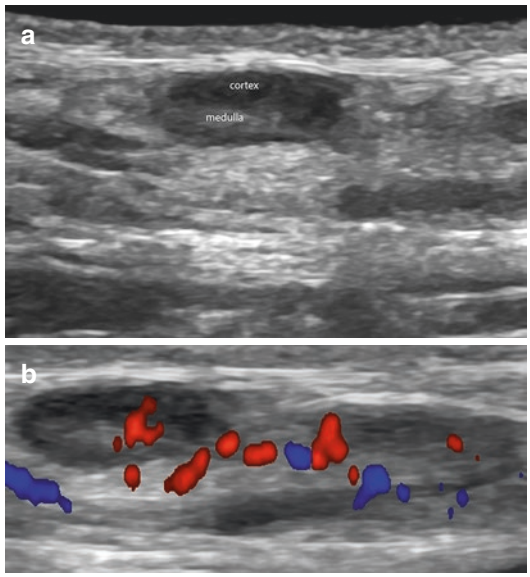

Fig. 5.13 Normal lymph node. (**a**) Grayscale and (**b**) color Doppler demonstrate an oval-shaped subcutaneous structure with a hypoechoic border (cortex) and a hyperechoic center (medulla). On color Doppler, notice the central distribution of the blood flow (in colors)

There are lymph node chains that should be studied when malignant or inflammatory dermatologic conditions are present [7, 9, 20].

Muscle

The muscles show a main hypoechoic structure with some hyperechoic lines in between the hypoechoic muscular fibers that correspond to fibrous septa. It is relevant to know the muscles' topographic anatomy and anatomical variants such as accessory muscles [9, 21] (Fig. 5.14).

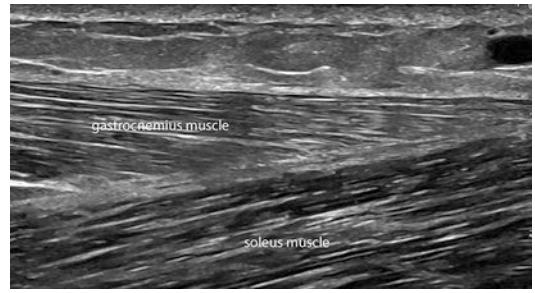

Fig. 5.14 Muscle. Notice the muscles' hypoechoic pattern that presents some hyperechoic fibrous septa between the muscular fibers

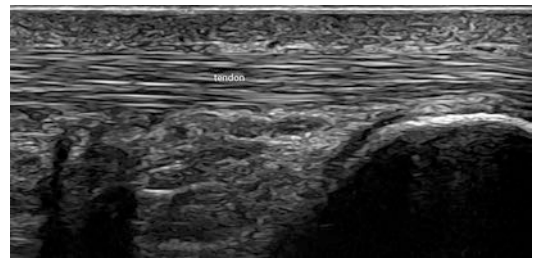

Fig. 5.15 Tendon. Hyperechoic fibrillar band corresponding to a tendon, in this case, the Achilles tendon in the ankle's posterior aspect

Tendons

The tendons are composed of collagen; therefore, they present a hyperechoic fibrillar pattern. Some accessory tendons should be recognized. They usually present a hypoechoic thin sheath except for some tendons, such as the Achilles tendon that shows a paratenon and not a real sheath [7, 9, 21, 22] (Fig. 5.15).

Joints

These present an anechoic space surrounded by the hyperechoic bony margins. It is common to detect a laminar amount of fluid of 1–2 mm in some joints, which should not be considered a pathological finding unless this feature is symptomatic and asymmetrical. It is useful for detecting abnormal fluid to explore the joints' lateral recesses, particularly in the hands and feet [7, 9, 21] (Fig. 5.16).

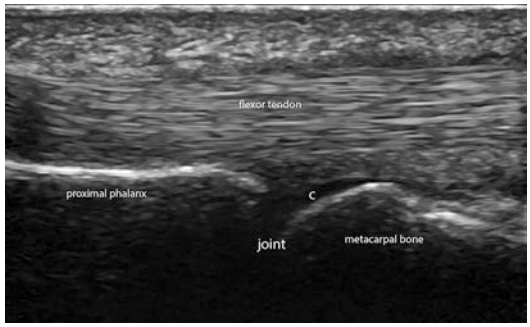

Fig. 5.16 Normal joint. Anechoic space between two bones. Notice an anechoic curved region attached to the distal epiphysis of the metacarpal that corresponds to the joint cartilage

Bursae

These saclike structures are intended to prevent the alteration of joints and tendons and present typical anatomical locations. Nevertheless, in some sites, neobursae can appear, particularly in the presence of chronic friction or trauma [7, 9, 21]. Under normal conditions, bursae are usually not detected (Fig. 5.17).

Nerves

They appear as mixed echogenicity structures with hypoechoic and hyperechoic longitudinal fibers. In the cross-sectional view, the nerves show as oval-shaped structures with hypoechoic and hyperechoic spots. Main nerves present well-known anatomical locations [7, 9, 21, 23] (Fig. 5.18).

Cartilage

It appears as a hypoechoic and well-defined band, usually with a wavy shape. The cartilage is avascular and receives nutrients from the peripheral tissues [7, 9, 21, 24] (Fig. 5.19).

Vessels

These are anechoic tubular structures that run in the skin layers. It is possible to detect a slightly

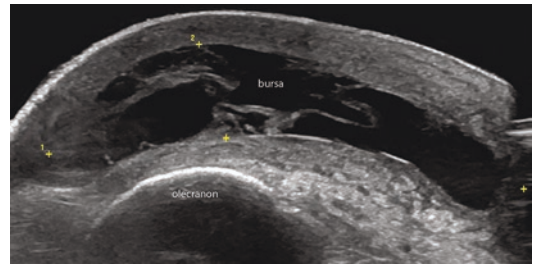

Fig. 5.17 Bursa. This is an inflammation of the olecranon bursa because the normal bursae are usually not possible to detect. Notice the anechoic saclike structure with some septa and echoes that correspond to the bursa (between markers)

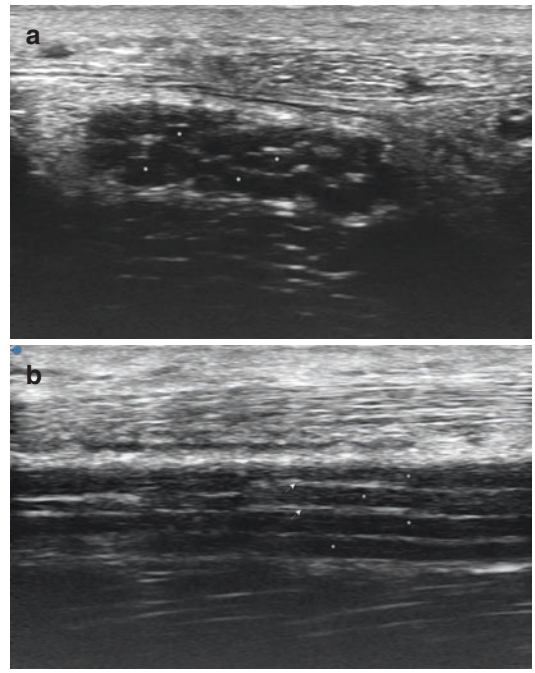

Fig. 5.18 Nerve (grayscale). (**a**) Transverse and (**b**) longitudinal views of the median nerve at 70 MHz. Notice the hypoechoic structure of the neural fascicles (*) and the hyperechoic septa (arrows) in-between the nerve bundles that correspond to the perineurium

hyperechoic line in the wall's inner parts of the main arteries that correspond to the intima. However, it would be difficult to observe the arterial vessels' intima in the cutaneous layers except for some vessels observed with 50–70 MHz. The spectral curve analysis presents the systolic and diastolic components of the flow. It is also possible to measure the peak sys-

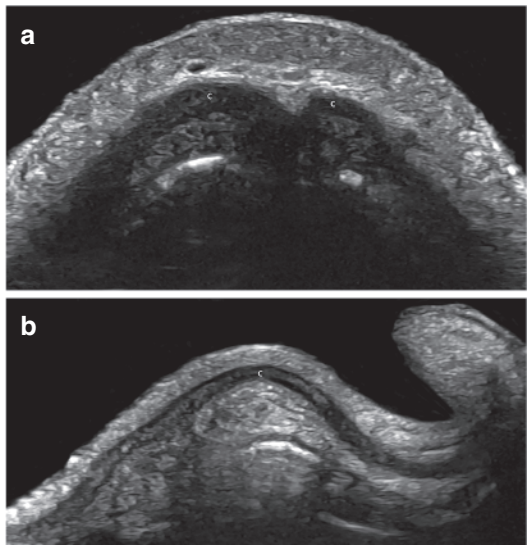

Fig. 5.19 Cartilage (c). (**a**) Nasal alar cartilages and (**b**) ear pinna cartilage. The normal cartilage appears as a deep hypoechoic structure with a soft wavy shape

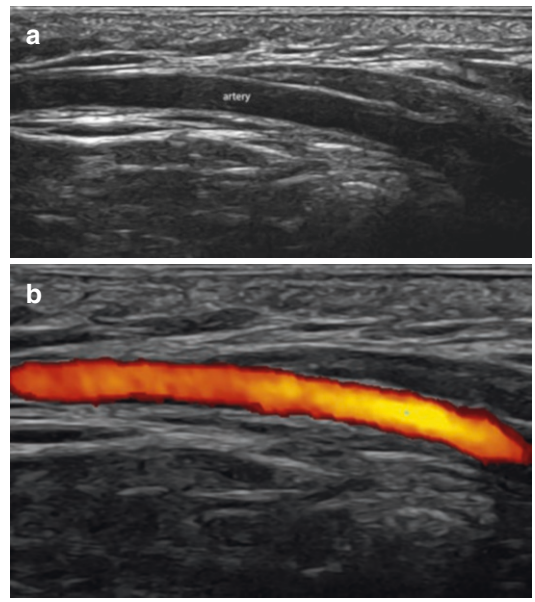

Fig. 5.20 Vessel. (**a**) Grayscale and (**b**) color Doppler of the temporal artery. The artery appears as an anechoic tubular structure. On color Doppler, there is blood flow (in color) within the vessel

tolic velocity of the arteries in cm/sec. The veins are usually compressible with the probe and present a monophasic type of flow [7, 9, 25, 26] (Fig. 5.20).

Glands

The most common glands prone to be involved in dermatologic pathology are the lacrimal, parotid, and submandibular glands. These usually appear as slightly hyperechoic structures with regular contours. The lacrimal gland vascularity is mainly supplied by the lacrimal artery, a branch of the internal carotid artery. The parotid glands' arterial blood flow comes from the posterior auricular and superficial temporal arteries, branches of the external carotid artery. In the case of the submandibular glands, the arterial vascularity comes from the submental and sublingual arteries, branches of the facial artery, and lingual artery.

There are minor salivary glands in the lip's submucosal layer that appear on ultrasound as round or oval-shaped hypoechoic structures.

Additionally, there are variants such as accessory glands commonly located on top of the upper third of the masseter muscle and that follow the parotid duct axis. Sometimes, the parotid gland also presents a prominent medial aspect covering the upper third of the masseter muscle. These variants are essential to know, particularly when the patient is exposed to facial procedures [7, 9, 27, 28] (Fig. 5.21).

Mammary Glands

The presence of ectopic fibroglandular mammary tissue may simulate soft-tissue lumps and bumps that can mimic some dermatologic lesions. This tissue is frequently found in the axillary regions, such as a prominent tail of the breast that reaches the axilla base or as an isolated axillary component. In men, the presence of fibroglandular mammary tissue in the areolar regions is called gynecomastia. On ultrasound, the fibroglandular

tissue presents a mixed echogenicity with hypoechoic and hyperechoic areas and is usually located in the subcutaneous layer. The balance between these components can vary from person to person, but we can compare the echostructure with the breasts' mammary tissue in a female patient.

There is also a ductal anechoic retroareolar system in the breast, which may not be seen in the ectopic locations [7, 9, 11] (Fig. 5.22).

Bone Calcium

The bony structure and the calcium deposits are hyperechoic and produce posterior acoustic shadowing artifacts. This is because the calcium tends to stop the passage of the sound waves. On ultrasound, the bones appear as hyperechoic lines and the deposits of calcium show as hyperechoic spots. In tiny deposits of calcium, the posterior acoustic shadowing artifact may not be so evident. The

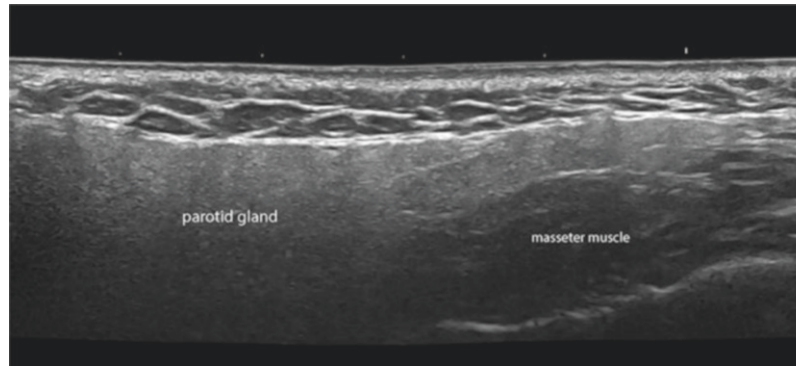

Fig. 5.21 Gland. Grayscale transverse view of the parotid gland. Notice the hyperechoic and homogenous structure of the gland

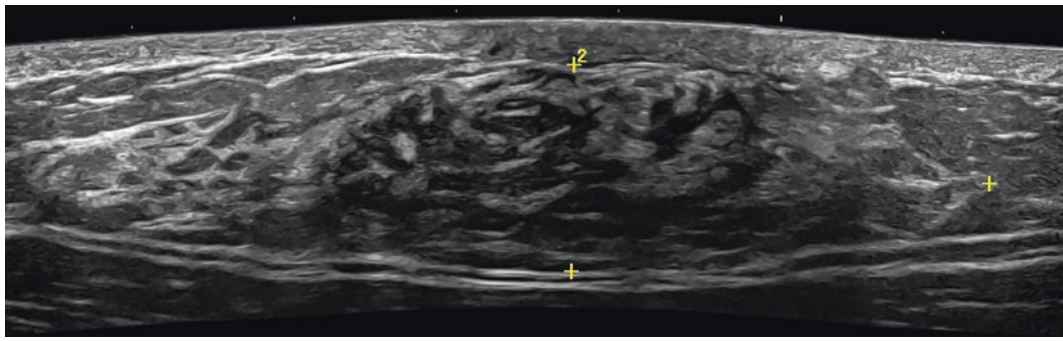

Fig. 5.22 Mammary gland. Notice the mixed echogenicity structure (between markers) that presents as hyperechoic and hypoechoic areas, which correspond to the fibroglandular mammary tissue

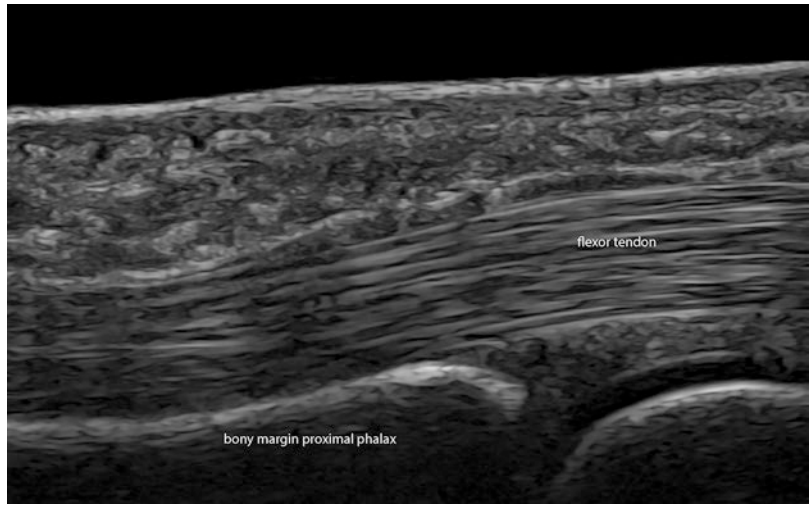

Fig. 5.23 Bone. The bone's cortex appears as a hyperechoic line that generates posterior acoustic shadowing artifact; in this case, the figure demonstrates the proximal phalanx's bony margin

increase of the frequency may support the posterior acoustic shadowing artifact's discrimination in small calcified structures [7, 9, 11, 29] (Fig. 5.23).

Conclusion

It is essential to know the normal anatomy of the skiny and adjacent structures to catch the abnormalities in the tissues.

References

1. Calonje E, Brenn T, Lazar A, Billings S. McKee's pathology of the skin. 5th ed. Amsterdam: Elsevier; 2019.
2. Kanitakis J. Anatomy, histology and immunohistochemistry of normal human skin. Eur J Dermatol. 2002;12(4):390–9; quiz 400–391.
3. McKee P, Calonje E, Granter S. The structure and function of skin. In: McKee P, Calonje E, Granter S, editors. Pathology of the skin with clinical correlations. Amsterdam: Elsevier/Mosby; 2005. p. 1–36.
4. Segura S, Requena L. Anatomy and histology of normal subcutaneous fat, necrosis of adipocytes, and classification of the panniculitides. Dermatol Clin. 2008;26(4).:419–424, v.
5. Wortsman X. Common applications of dermatologic sonography. J Ultrasound Med. 2012;31(1):97–111.
6. Wortsman X. Ultrasound in dermatology: why, how, and when? Semin Ultrasound CT MR. 2013;34(3):177–95.
7. Wortsman X. Atlas of dermatologic ultrasound. 1st ed. New York, NY: Springer International Publishing; 2018.
8. Wortsman X, Carreno L, Ferreira-Wortsman C, et al. Ultrasound characteristics of the hair follicles and tracts, sebaceous glands, Montgomery glands, apocrine glands, and Arrector pili muscles. J Ultrasound Med. 2019;38(8):1995–2004.
9. Wortsman X, Jemec GBE. Dermatologic ultrasound with clinical and histologic correlations. 1st ed. New York, NY: Springer-Verlag New York; 2013.
10. Wortsman X, Wortsman J. Clinical usefulness of variable-frequency ultrasound in localized lesions of the skin. J Am Acad Dermatol. 2010;62(2):247–56.
11. Wortsman X, Wortsman J, Carreño L, Morales C, Sazunic I, Jemec G. Sonographic anatomy of the skin, appendages and adjacent structures. In: Wortsman

X, Jemec G, editors. Dermatologic ultrasound with clinical and histologic correlations. 1st ed. New York: Springer; 2013. p. 15–35.
12. Gniadecka M, Gniadecki R, Serup J, Søndergaard J. Ultrasound structure and digital image analysis of the subepidermal low echogenic band in aged human skin: diurnal changes and interindividual variability. J Invest Dermatol. 1994;102(3):362–5.
13. Mandava A, Ravuri PR, Konathan R. High-resolution ultrasound imaging of cutaneous lesions. Indian J Radiol Imaging. 2013;23(3):269–77.
14. Schneider MR, Schmidt-Ullrich R, Paus R. The hair follicle as a dynamic miniorgan. Curr Biol. 2009;19(3):R132–42.
15. Wortsman X, Wortsman J, Matsuoka L, et al. Sonography in pathologies of scalp and hair. Br J Radiol. 2012;85(1013):647–55.
16. Aluja Jaramillo F, Quiasúa Mejía DC, Martínez Ordúz HM, González AC. Nail unit ultrasound: a complete guide of the nail diseases. J Ultrasound. 2017;20(3):181–92.
17. Cecchini A, Montella A, Ena P, Meloni GB, Mazzarello V. Ultrasound anatomy of normal nails unit with 18 MHz linear transducer. Ital J Anat Embryol. 2009;114(4):137–44.
18. Rodriguez-Takeuchi SY, Villota V, Renjifo M. Anatomy and pathology of the nail and subungual space: imaging evaluation of benign lesions. Clin Imaging. 2018;52:356–64.
19. Wortsman X, Jemec GB. Ultrasound imaging of nails. Dermatol Clin. 2006;24(3):323–8.
20. Loh Z, Hawkes EA, Chionh F, Azad A, Chong G. Use of ultrasonography facilitates noninvasive evaluation of lymphadenopathy in a lymph node diagnostic clinic. Clin Lymphoma Myeloma Leuk. 2021;21(2):e179–84.
21. van Holsbeeck M, Introcaso J. Musculoskeletal ultrasound. 3rd ed. New Delhi: Jaypee Brothers; 2016.
22. Rasmussen OS. Sonography of tendons. Scand J Med Sci Sports. 2000;10(6):360–4.
23. Propeck T, Quinn TJ, Jacobson JA, Paulino AF, Habra G, Darian VB. Sonography and MR imaging of bifid median nerve with anatomic and histologic correlation. AJR Am J Roentgenol. 2000;175(6):1721–5.
24. Wortsman X, Jemec GB. Sonography of the ear pinna. J Ultrasound Med. 2008;27(5):761–70.
25. Gaitini D. Multimodality imaging of the peripheral venous system. Int J Biomed Imaging. 2007;2007:54616.
26. Gaitini D, Soudack M. Diagnosing carotid stenosis by Doppler sonography: state of the art. J Ultrasound Med. 2005;24(8):1127–36.
27. Hiyama T, Kuno H, Sekiya K, Oda S, Kobayashi T. Imaging of malignant minor salivary gland tumors of the head and neck. Radiographics. 2021;41(1):175–91.
28. Straughan AJ, Badger CD, Benito DA, Joshi AS. Salivary gland ultrasound training: improving anatomic identification in residents. Am J Otolaryngol. 2020;41(6):102734.
29. Wortsman X, Claveria P, Valenzuela F, Molina MT, Wortsman J. Sonography of acne vulgaris. J Ultrasound Med. 2014;33(1):93–102.